RSC Advances

PAPER

Cite this: *RSC Adv.*, 2019, **9**, 42430

$Cs_4PbBr_6/CsPbBr_3$ perovskite composites for WLEDs: pure white, high luminous efficiency and tunable color temperature

Shangxuan Huang,[a] Sen Yang,[a] Qi Wang,[a] Ruirui Wu,[a] Qiuju Han[b] and Wenzhi Wu *[a]

Received 5th December 2019
Accepted 15th December 2019

DOI: 10.1039/c9ra10183g

rsc.li/rsc-advances

$Cs_4PbBr_6/CsPbBr_3$ perovskite composites are fabricated by room-temperature one-pot mixing synthesis, which is short in time, free from inert gases and delivers a high product yield. Temperature-dependent photoluminescence shows that a larger exciton binding energy of 291.1 meV exhibits better thermal stability compared with that of pure Cs_4PbBr_6 and $CsPbBr_3$ materials. The CIE chromaticity coordinates (0.1380, 0.7236) of green LEDs designed with $Cs_4PbBr_6/CsPbBr_3$ perovskite composites show almost no variation under driving current changing from 5 to 30 mA. Furthermore, the ground $Cs_4PbBr_6/CsPbBr_3$ perovskite composites mixed with red emitting $K_2SiF_6:Mn^{4+}$ phosphor are dropped and casted on a blue-emitting InGaN chip. The white light emitting diodes (WLEDs) are presented, which have good luminous efficiency of 65.33 lm W^{-1} at 20 mA, a correlated color temperature of 5190 K, and the white gamut with chromaticity coordinate of (0.3392, 0.3336). According to the state of art, these excellent characteristics observed are much superior to the reported results of conventional perovskite-based WLEDs, which demonstrate the immense potential and great prospect of $Cs_4PbBr_6/CsPbBr_3$ perovskite composites to replace conventional phosphors in lighting devices.

1 Introduction

An increasing awareness of the necessity for energy conservation has directed scientific research to develop various energy-saving materials and techniques for use in displays and lighting applications.[1] In this context, white light emitting diodes (WLEDs) promise great potential to replace traditional incandescent white light sources because of their significantly economic and technological advantages in energy conservation. On all counts, commercial WLEDs have been adopted as a combination of an InGaN blue chip with a YAG: Ce^{3+} yellow phosphor.[2] The red and green phosphors are used to realize a high color rendering index and color tuning with adding red and green phosphors for trichromatic LEDs.[3] Traditional phosphors, delivering up to 150–230 lm W^{-1} of luminous efficiency LEDs,[4] rely solely on using combinations of rare-earth ions.[5,6] The use of these rare-earth based phosphors is restricted by some intrinsic optical defects, limited and hard preparation conditions, high cost, toxicity and pollution in mining and refining, as well as the requirement of limited resource.[7,8] Accordingly, an immense and challenging assignment concernful to modern solid-state lighting is the discovery of highly efficient phosphors free of rare-earth elements.[9]

Recently, luminescent metal-halide perovskite semiconductors have attracted enormous attention owing to their excellent optoelectronic properties such as high quantum yield,[10,11] chromatogram purity,[12] wide wavelength (400–800 nm) tunability and narrow emission linewidth,[13,14] which enable them to achieve promising applications in phosphor-converted LEDs,[15,16] solar cells[17,18] and photodetectors.[19,20] Among them, cesium lead bromine has emerged as a promising optoelectronic material and attracted an enormous amount of interests. It is a medium-bandgap semiconductor which can be synthesized cost-effectively on large scales through simple solution-based processes.[21,22] In particular, the rapid advances in perovskite materials are drawn significant attention to nanocrystals (NCs) based on the perovskite for use in WLEDs. For example, both $CsPbBr_3$ NCs[23] and $Cs_4PbBr_6/CsPbBr_3$ nanocomposites[24] as the visible color emitting materials are combined with a blue LED chip and conventional phosphors such as $CaAlSiN_3:Eu^{2+}$. Unfortunately, colloidal $CsPbBr_3$ NCs are found to show relatively poor thermal stability because of the damage of ligands and the ensuing particle aggregation or fusion at elevated temperature, reflected by the rapid PL quenching and ripening of the NCs.[25] $CsPbBr_3$ NCs imbedded in a Cs_4PbBr_6 host matrix achieve photoluminescence quantum yield (PLQY) up to 90% (ref. 26) in contrast to very low light yield from bulk single crystal or polycrystalline $CsPbBr_3$.[27] The thermal stability of PL for $CsPbBr_3$ NCs is enhanced due to the passivation of Cs_4PbBr_6 host matrix.[24,28] In these senses,

[a]*School of Electronic Engineering, Heilongjiang University, Harbin, Heilongjiang, 150080, China. E-mail: wuwenzhi@hlju.edu.cn*

[b]*School of College of Arts and Sciences, Northeast Agricultural University, Harbin, Heilongjiang, 150030, China*

$Cs_4PbBr_6/CsPbBr_3$ perovskite composites are promising candidates to replace ordinary phosphors for future solid-state lighting technology. The optical performance of these perovskites is impressive, several challenging issues, such as the ability to perform large-scale synthesis as well as the product yield, remain inevitable obstructions for practical applications in optoelectronic devices. Furthermore, in the WLEDs working process, the influence of operating time and driving current is obvious. Although the luminous efficiency and CIE coordinates of perovskite-based WLEDs are reported, to the best of our knowledge, there are no comprehensive reported on parameters in these regards.

In this work, we use a facile and rapid approach for the synthesis of high-yield $Cs_4PbBr_6/CsPbBr_3$ perovskite composites at room temperature. The strong green PL from $Cs_4PbBr_6/CsPbBr_3$ composites is observed, and the characterization and temperature-dependent PL of them are investigated. Here, pure and stable WLED devices are fabricated by combining the highly luminescent $Cs_4PbBr_6/CsPbBr_3$ composites as green emitters and commercial $K_2SiF_6:Mn^{4+}$ phosphors as red emitters with blue-emitting InGaN chips. Moreover, the optoelectronic characteristics of the WLEDs under different driving current and treating time are investigated in detail.

2 Experimental technique

2.1 Materials and chemicals

Lead bromide ($PbBr_2$, 99%, Macklin), cesium acetate (CsAc, 99%, Aladdin), HBr water solution (48% by weight in H_2O, Macklin), Dimethyl sulfoxide (DMSO, 99.8%, Macklin), $K_2SiF_6:Mn^{4+}$, silicone gel A and B, and blue LED chip (460 nm, 1 W, looking long). All of these chemicals are used without any further purification.

2.2 Preparation of perovskite composites

Here, the perovskite composites are prepared based on the modified one-pot mixing method through the reaction of CsAc and $PbBr_2$ powder in DMSO with aqueous HBr solution.[29] In detail, 0.22 mmol of $PbBr_2$ and 0.88 mmol of CsAc are dissolved in 0.9 mL of DMSO, which are stirred in a closed beaker for 30 minutes at room temperature to form the precursor solution. Then, 0.1 mL of aqueous HBr solution is slowly injected into the precursor solution to induce the reaction *via* stirring. Limited by the solubility of CsBr in DMSO, in order to obtain a higher concentration of precursor solution, we use CsAc with higher solubility instead of CsBr as the Cs source and $PbBr_2$ as the Pb source. Meanwhile, aqueous HBr solution is used to make up for the deficiency of Br in CsAc. Immediately, yellow-green precipitates can be observed in the mixed solution, which is stirred 6 h at room temperature. The precipitation is separated from the mixed solution by centrifugation at 4000 rpm for 5 minutes and washed once with 0.2 mL DMSO. After this purification process, the powder is collected and dried at 50 °C for 12 h under vacuum. The solvent (DMSO) used in this work is 0.9 mL unless otherwise noted.

2.3 Construction of WLEDs

The perovskite composites are used as phosphors to fabricate WLEDs. A blue LED chip, emitting at 460 nm, is attached on the bottom of the reflector cup by using conductive silver paste. In a typical procedure, 0.05 g perovskite composites with peak wavelength centered at 521 nm are mixed with 0.05 g $K_2SiF_6:Mn^{4+}$ phosphors emitting at 630 nm, then mixing them with 1 mL silicone gel A and B (0.2 mL of A, 0.8 mL of B). Afterward, removing the bubbles in the silicone gel in a vacuum chamber and overcoating the mixture on the chip. After that, capping the reflector cup with an optical lens. Finally, the chip is dried at 50 °C for 2 h.

2.4 Characterization

Powder X-ray diffraction (XRD) pattern is recorded with a powder diffractometer (Dmax2500, Rigaku) using Cu Kα radiation ($\lambda = 0.154$ nm). Photoluminescence (PL) spectra are recorded on a spectrometer (HR4000CG-UV-NIR, Ocean Optics). The temperature-related PL of $Cs_4PbBr_6/CsPbBr_3$ composites is evaluated using a vacuum liquid-nitrogen cryostat (Cryo-77, Oriental Koji) and a continuous-wave (CW) laser (UV-FN-405-200 mW, CNI) at 405 nm with the capability to give the temperature variation from 100 to 400 K. The PL dynamics are excited by 200 ps laser pulses at 450 nm and measured by a time-correlated single photon counting (TCSPC) system from Boston Electronics with the time resolution of 200 ps to reveal the process of exciton recombination. Photoelectric parameters including electroluminescence (EL) spectra, luminous efficiency (LE), color rendering index (CRI), correlated color temperature (CCT), and Commission Internationale de L'Eclairage (CIE) chromaticity coordinates are evaluated using the spectrometer connected to an integrating sphere (HP30, Hopoo) with an optical fiber under the different operating current.

3 Results and discussions

3.1 Synthesis and characterization of $Cs_4PbBr_6/CsPbBr_3$ composites

Herein, we use a one-pot reaction strategy to realize the high yield room temperature synthesis of novel perovskite-related $Cs_4PbBr_6/CsPbBr_3$ semiconductors. As shown in Fig. 1a, the high product yield of 86.2%, 80.1%, 70.9%, 67.5%, and 59.3% are obtained by adding different amounts (0.6, 0.7, 0.8, 0.9, 1.0 mL, respectively) of DMSO solvent. It's commonly known that DMSO is a good solvent for $CsPbBr_3$ NCs but not for micron-sized Cs_4PbBr_6, so after washing with DMSO, the precipitation is $Cs_4PbBr_6/CsPbBr_3$ perovskite composites.[30] The possible conversion reactions can be the following:

$$PbBr_2 + 4CsAc + 4HBr \rightarrow Cs_4PbBr_6 \quad (1)$$

$$PbBr_2 + CsAc + HBr \rightarrow CsPbBr_3 \text{ (rarely, embedded in } Cs_4PbBr_6) \quad (2)$$

Only the micron-sized Cs_4PbBr_6 and the very small amount of nano-sized $CsPbBr_3$ embedded therein exists in the target product, which makes it easy for us to calculate the yield by element conservation of lead and assuming that the obtained product is all Cs_4PbBr_6. Here, we emphasize again that this approach of synthesizing perovskites has a high yield, which can be calculated using the following equation, certainly indicating its promising applications in the industry field.

$$\text{Yield} = \frac{\text{Actual production}}{\text{Theoretical production}} \quad (3)$$

The perovskite composites are characterized using the scanning electron microscope (SEM), which shows irregular morphology and size of $Cs_4PbBr_6/CsPbBr_3$ perovskite composites on the micrometer scale as shown in Fig. 1b. The inset is observed on 200 nm scale to study more detailed structures. Fig. 1c shows the X-ray diffraction (XRD) pattern of the resulting composites powder. The XRD pattern of the sample matches well with that of rhombohedral Cs_4PbBr_6 crystals with no obvious difference observed. It should be noted that the unavoidable coexistence of $CsPbBr_3$ NCs with Cs_4PbBr_6 crystals and the detection limit of XRD measurements is about 5 wt%, the content of $CsPbBr_3$ NCs in $Cs_4PbBr_6/CsPbBr_3$ composites can't be accurately measured. Consequently, further discussion is much needed to clarify the origin of highly green emission in zero-dimensional Cs_4PbBr_6 crystals. To our knowledge, no explanation is given for the absorption in the green region for supposedly pure Cs_4PbBr_6.[31] The extreme similarity of wide bandgap Cs_4PbBr_6 green emission with that of $CsPbBr_3$ NCs, and the green PL in Cs_4PbBr_6 is often reported to have a very narrow FWHM, this narrow PL matches that of $CsPbBr_3$ NCs. It is believed that the embedded $CsPbBr_3$ NCs are responsible for the highly efficient PL. This viewpoint is further strengthened by direct imaging of $CsPbBr_3$ NCs in Cs_4PbBr_6.[32] In the PL spectrum of the $Cs_4PbBr_6/CsPbBr_3$ composites, a narrow emission band centered at 521 nm (2.38 eV) with the full width at half maximum (FWHM) of 25 nm (116 meV) are observed at 290 K as seen in Fig. 1d. The result obtained for PL spectrum is similar to $CsPbBr_3$ NCs.[33] UV-vis absorption spectrum of the composites shows that absorption onset at 550 nm and a strong absorption peak at 310 nm. Moreover, the PLQY of $Cs_4PbBr_6/CsPbBr_3$ perovskite composites is determined using a spectrofluorometer equipped with an integrating sphere under the excitation of 365 nm illumination. The result of 32% is obtained for the product when the volume of the solvent (DMSO) is 0.9 mL.

3.2 Photophysical properties of $Cs_4PbBr_6/CsPbBr_3$ composites

To explore the PL mechanism of $Cs_4PbBr_6/CsPbBr_3$ perovskite composites, temperature-dependent PL spectra are recorded at the temperature ranging from 100 to 400 K as seen in Fig. 2a. The PL peak at 100 K is as narrow as 13.5 nm and exhibits a temperature-sensitive evolution, *i.e.*, monotonously decreases as the temperature is elevated. The important physical parameter of exciton binding energy, which is vital for excitation and recombination processes of semiconductors, can be estimated according to temperature-dependent PL behavior using Arrhenius equation:[34]

$$I(T) = \frac{I_0}{1 + A\, e^{-E_b/k_B T}} \quad (4)$$

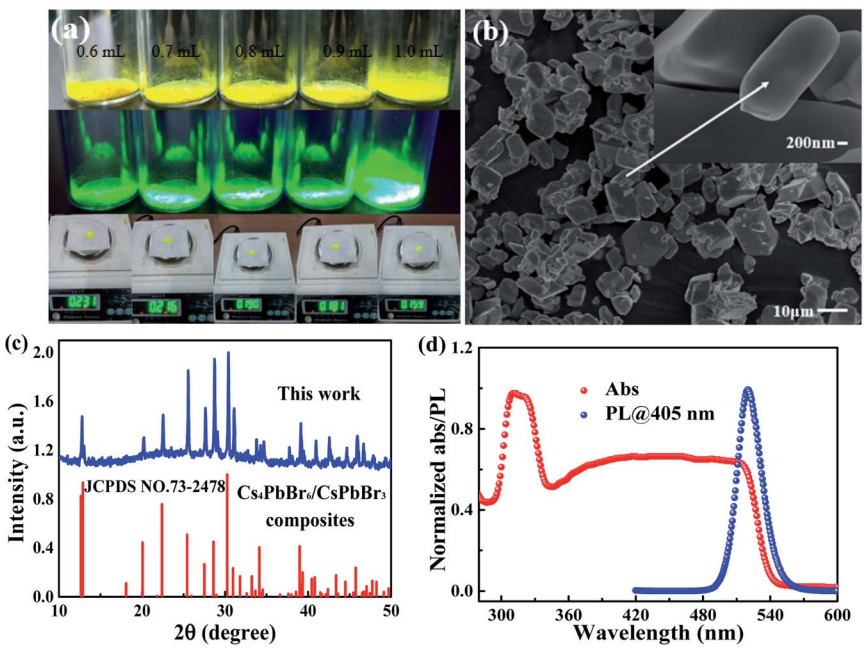

Fig. 1 (a) Images of the $Cs_4PbBr_6/CsPbBr_3$ perovskite composites under daylight (top) and UV light (365 nm) (middle). The bottom from left to right is the product yield of 86.2%, 80.1%, 70.9%, 67.5%, 59.3%, respectively. (b) SEM image, (c) XRD pattern and (d) absorption, PL spectra of $Cs_4PbBr_6/CsPbBr_3$ perovskite composites.

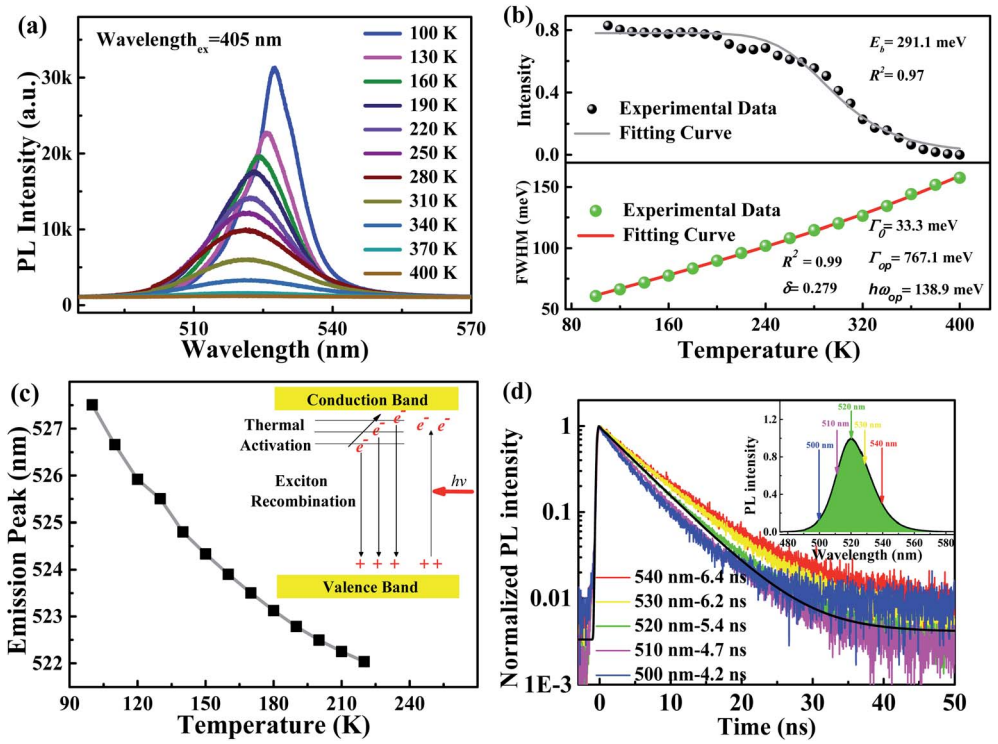

Fig. 2 (a) Temperature-dependent PL spectra of Cs_4PbBr_6/$CsPbBr_3$ perovskite composites. (b) Integrated PL emission intensity (top), FWHM (bottom). (c) Emission peak as a function of temperature, the inset shows the related process of a thermally-induced exciton emission blue-shift. (d) Wavelength-dependent time-resolved PL.

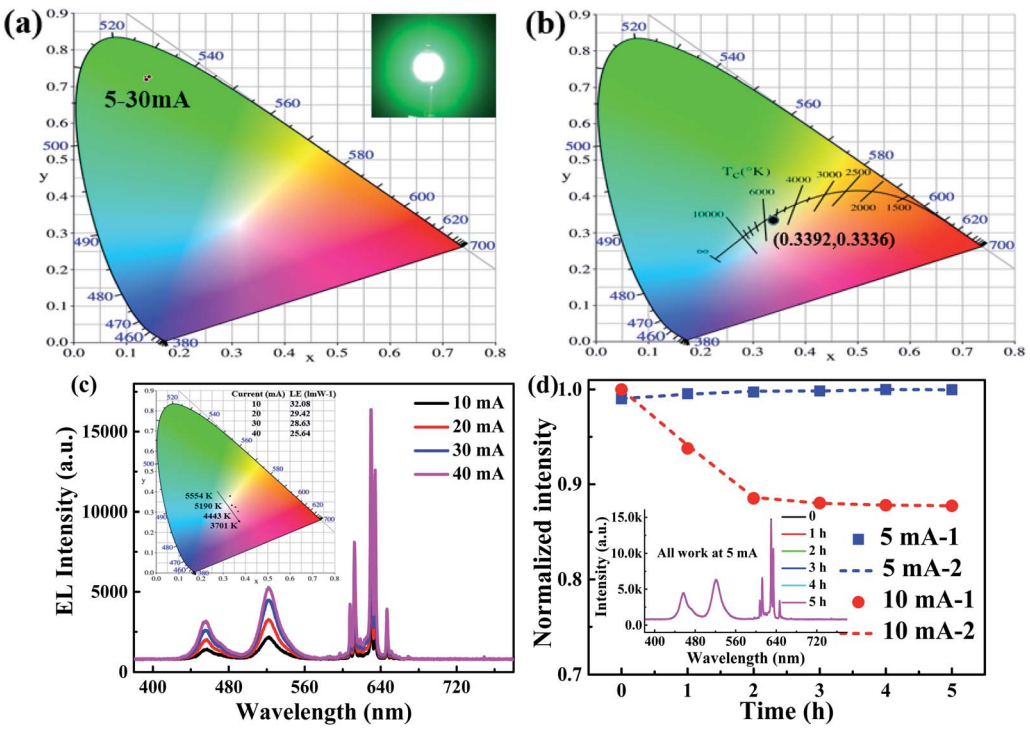

Fig. 3 (a) CIE coordinates of the green pero-LEDs, the inset shows the related photograph of the working LED. (b) Optimized CIE chromaticity coordinates of pero-WLEDs. (c) EL spectra of the constructed pero-WLEDs operated under different driving current, the inset shows overall luminous characteristics at 20 mA. (d) The changes of EL integrated intensity of green band in pero-WLEDs at 5 and 10 mA, respectively. The short dash and square symbols represent our repetitive experiments to increase reliability. The inset shows the EL spectra of the constructed pero-WLEDs operated under 5 mA, which has barely changed within five hours.

where $I(T)$ and I_0 are the integrated PL intensities at temperature T and 0 K, respectively, E_b is the exciton binding energy, and k_B is the Boltzmann constant. The corresponding exciton binding energy of $Cs_4PbBr_6/CsPbBr_3$ perovskite composites is experimentally obtained as 291.1 meV in Fig. 2b, which is higher than pure $CsPbBr_3$ and Cs_4PbBr_6 crystal,[35] and close to that of similar $Cs_4PbBr_6/CsPbBr_3$ composites,[36] Such a large exciton binding energy confirms that PL of $Cs_4PbBr_6/CsPbBr_3$ perovskite composites mainly occurs through exciton recombination rather than free carrier recombination.[37] Interestingly, a significant broadening of the FWHM is observed with an increase of temperature as shown in Fig. 2b, which can be fitted as:[28]

$$\Gamma(T) = \Gamma_0 + \sigma T + \frac{\Gamma_{op}}{e^{\hbar\omega_{op}/k_B T} - 1} \quad (5)$$

where $\Gamma(T)$ is the FWHM at temperature T, and Γ_0 is the inhomogeneous broadening contribution, which is ascribed to the scattering of excitons by defects or doped carriers and is temperature-independent. σ and Γ_{op} are the coupling coefficients of exciton-acoustic phonon and exciton-optical phonon, respectively. The fitting result is shown in Fig. 2b, which indicates that the optical phonon is dominant for the exciton–phonon interactions in the present $Cs_4PbBr_6/CsPbBr_3$ perovskite composites. Accordingly, the optical phonon energy ($\hbar\omega_{op}$) involved in the exciton recombination is determined to be 138.9 meV, confirming strong exciton–phonon interactions and weak nonradiative transition for exciton recombination. Finally, an obvious blue-shift of the emission peak position is observed during the temperature increasing from 100 to 220 K as shown in Fig. 2c. It is well known that the excitons will occupy a lower discrete energy state below the conduction band at low temperature. As the temperature is elevated, electrons may migrate from lower energy states to higher ones with the assistance of phonons, resulting in a blue shift in the emission band.[38] The related process is shown in the inset of Fig. 2c. But when the temperature gradually from 220 rises to 400 K, the emission band of $Cs_4PbBr_6/CsPbBr_3$ perovskite composites remains steady. This reveals that composites are less sensitive to relatively high temperature. To further unravel the excitonic recombination mechanism, wavelength-dependent time-resolved PL of $Cs_4PbBr_6/CsPbBr_3$ perovskite composites are performed. Based on nonlinear least squares fitting, the measured PL decays are fitted and calculated. It can be seen from Fig. 2d that the exciton PL decays are single-exponential, indicating the existence of one emission centers in $Cs_4PbBr_6/CsPbBr_3$ perovskite composites. As is commonly known, the morphology and the size of crystals influence their optical properties.[39] The lifetime decay component becomes longer from 4.2 to 6.4 ns with the change of detection wavelength from 500 to 540 nm, which exhibits the PL lifetime increases steadily with increasing NCs size embedded in Cs_4PbBr_6 microcrystals consistent with the reported $CsPbBr_3$ NCs.[40]

3.3 Applications of $Cs_4PbBr_6/CsPbBr_3$ composites on WLEDs

In order to study the color stability of perovskite materials, the ultraviolet LEDs with the peak emission at 360 nm and $Cs_4PbBr_6/CsPbBr_3$ perovskite composites are used to fabricate green perovskite LEDs (green pero-LEDs). The CIE chromaticity coordinates of the green pero-LEDs (0.1380 ± 0.0035, 0.7236 ± 0.0026) are overlapped as displayed in Fig. 3a, and no obvious change with the increasing driving current (5–30 mA), indicating greater color stability of output light.

From the viewpoint of application exploration, the strong PL emission and color stability from $Cs_4PbBr_6/CsPbBr_3$ perovskite composites are inspired their use in light-emitting applications. EL spectra of perovskite WLEDs (pero-WLEDs) under various driving current are indicated in Fig. 3c, showing three peaks centered at 460, 521 and 630 nm, corresponding to the emission of blue LED chip, $Cs_4PbBr_6/CsPbBr_3$ perovskite composites and $K_2SiF_6:Mn^{4+}$ phosphors, respectively. Blue and green-red emission intensities steadily raise with increased current, revealing that LEDs had stable light-conversion and color quality. The optical parameters of pero-WLEDs at different driving current are shown in the inset of Fig. 3c. With increase in driving current, the CCT of pero-WLEDs is changed from 5554 to 3701 K. Although a slight decrease in luminous efficiency from 32.08 to 25.64 lm W^{-1} is observed when driving current increases from 10 to 40 mA. After optimization, the maximum luminous efficiency of 65.33 lm W^{-1} at 20 mA can be obtained by changing the mass ratio of perovskites and $K_2SiF_6:Mn^{4+}$ on 1 : 2 (in detail, 0.05 g of $Cs_4PbBr_6/CsPbBr_3$ perovskite composites, 0.10 g of $K_2SiF_6:Mn^{4+}$, both are uniformly mixed in 1 mL of silicone gel A and B (0.2 mL of A, 0.8 mL of B)). These results show that the white light generated from the pero-WLEDs has high color chromatics stability against the increase of driving current, which is consistent with the high photostability of our perovskite materials. We do know that the device performance is comparable to some states of the art WLEDs based on conventional perovskite MCs or NCs, which are summarized and compared with other research groups as shown in Table 1. First, such high luminous efficiency is inseparable from the high PLQY of the product, work has reported that the latter can be further improved by optimizing perovskites structure such as doping of lanthanide ions[41] or forming a quasi core/shell structure.[42] Second, the PL line-widths of our product are

Table 1 Parameter comparisons of WLEDs based on $Cs_4PbBr_6/CsPbBr_3$ perovskite composites and conventional perovskite MCs/NCs-based LEDs

Emitting materials	LE (lm W^{-1})	CIE coordinate	References
Mn-doped $CsPbBr_{0.5}I_{2.5}$ NCs	29.7	(0.3327, 0.3688)	43
Cs_4PbBr_6 MCs	9.79	(0.3623, 0.3765)	12
Cs_4PbBr_6 MCs	13.91	(0.2879, 0.2434)	44
$CsPbBr_3$ NCs	—	(0.33, 0.30)	23
$CH_3NH_3PbBr_3/NaNO_3$	22.39	(0.28, 0.32)	45
$CH_3NH_3PbBr_3$@POSS	38	(0.30, 0.33)	46
$CsPbBr_3$@NH_4Br	—	(0.36, 0.35)	47
$CsPbBr_3$ NCs	—	(0.33, 0.36)	48
CsPb $(Br/I)_3$/POSS	14.1	(0.35, 0.38)	49
$CH_3NH_3PbBr_3/SiO_2$	60.5	(0.26, 0.25)	50
$CH_3NH_3PbX_3$ NCs/SiO_2	61.2	(0.33, 0.33)	51
$Cs_4PbBr_6/CsPbBr_3$	65.33	(0.3392, 0.3336)	This work

Table 2 Overall luminous characteristics with different treating time at 20 mA

Time (h)	LE (lm W^{-1})	CRI	CCT (K)	CIE coordinate
0	30.40	63.1	5256	(0.3379, 0.3369)
1	30.29	63.8	5014	(0.3392, 0.2876)
2	29.41	62.1	4555	(0.3442, 0.2742)
3	28.42	60.3	4375	(0.3454, 0.2671)
4	28.27	54.3	4253	(0.3461, 0.2632)

obviously narrower, which is significant for wide color-gamut display. Third, as we known that the CIE coordinates accurately represent the color of the light source, when mass ratio of Cs_4PbBr_6/$CsPbBr_3$ perovskite composites and K_2SiF_6:Mn^{4+} is between 1 : 2 and 1 : 3, optimized color coordinates is generated and reached (0.3392, 0.3336) at 20 mA as shown in Fig. 3b, this value of CIE is almost equal to the standard white light (0.33, 0.33). Last but not the least, high-quality Cs_4PbBr_6/$CsPbBr_3$ perovskite composites can be formed at room temperature even relatively low temperature, within short time, free from inert gas and injection operation.

Optical stability under operation time is one of the key factors to evaluate the performance of a light emitting device. From Fig. 3d, the EL intensity of the pero-WLEDs still maintains stability of the initial value after 5 h of continuous operation at 5 mA. When the driving current reaches 10 mA, its relative emission intensity declines slowly to 88% after 2 h and then tends to remain constant. In order to further explore the optical performance of pero-WLEDs after working for a period of time. The result in Table 2 illustrates the luminous efficiency dropped by only ~7% after 4 h of operation at 20 mA, the CIE color coordinate and CCT show the changes from (0.3379, 0.3369) to (0.3461, 0.2632) and 5256 to 4253 K, respectively. Because more current addition will cause mixture stronger emitting of the red *versus* blue color, and relatively weaker green color in WLEDs due to loss green light. These results demonstrate the highly optical stability of the pero-WLEDs at low current. Additionally, the CRI is measured for this WLEDs with warm perception. It is approximately 60 dues to the deficiency in yellow wave band, and we believe it can be improved further after optimization over the concentrations of phosphors or used the phosphor with a wider band[52] in the WLEDs.

Obviously, the color temperature of these WLEDs can be tuned through controlling the composites ratio of green and red components. To confirm the change of white target, the Cs_4PbBr_6/$CsPbBr_3$ phosphor is composited with K_2SiF_6:Mn^{4+} phosphor with the mass ratio of 1 : *x* (1 : 0, 1 : 0.5, 1 : 1, 1 : 2, 1 : 3 and 1 : 4) as shown in Fig. 4a. With an increasing composite ratio, generated warm-white light due to the addition of the red component, this perfect combination of green and

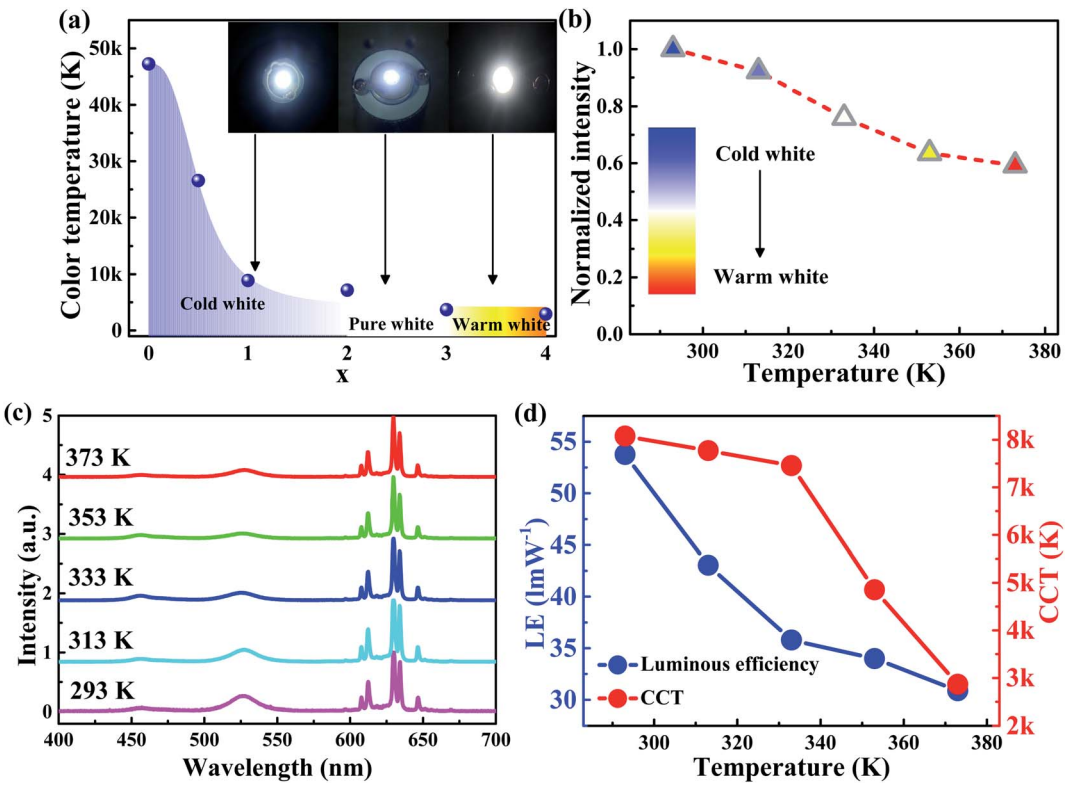

Fig. 4 (a) Color temperatures of pero-WLEDs as a function of mass ratio of green-to-red materials, where *x* comes from 1 : *x*. The insets show the related photograph of the working WLEDs. (b) Normalized intensity of green emission peak of the constructed pero-WLEDs operated under different drying temperature of silicone gel and phosphors. (c) EL spectra operating at different temperatures. (d) The changes of LE and CCT with drying temperature.

red components is suitable for lighting technology. These results indicate that the relatively low intensity of green color compared to that of red color is suitable for a warm color. And the intensity of green should be stronger to achieve a cool color.

Considering the sensitivity of the perovskite materials to heat, degrees raise in temperature would be remarkably influenced for the stability of the perovskites. As we change the drying temperature of silicone gel and phosphors from 293 to 373 K and keeping the drying time for 2 h, the integrated intensity of the green emission peak of pero-WLEDs decreases as shown in Fig. 4b. Fig. 4c is the EL spectra operating at temperatures 293, 313, 333, 353, 373 K, respectively. We know that perovskite materials are generally unstable at high temperatures, with increasing temperature, the thermal distribution will become worse as more non-emissive NCs generation around could hinder the thermal re-emission. From Fig. 4d, the luminous efficiency of pero-WLEDs decreases from 53.76 to 30.88 lm W^{-1} and CCT from 8077 to 2866 K at 20 mA on account of the unstable characteristics of the $Cs_4PbBr_6/CsPbBr_3$ perovskite composites at high temperature.

4 Conclusion

In summary, the $Cs_4PbBr_6/CsPbBr_3$ perovskite composites are synthesized using a one-pot mixing method, and boast large-scale production possibility. The prepared perovskites show the behavior of excellent luminous properties (PLQY = 32%) with narrow FWHM (25 nm) and large binding energy of 291.1 meV. The optimal device for WLEDs shows favorable white light characteristics with the CIE coordinates, CCT and LE of (0.3392, 0.3336), 5190 K and 65.33 lm W^{-1}, respectively. What is more, excellent optical stability is demonstrated with increasing driving current from 10 to 40 mA. And high device stability is also proved after working 5 h. More importantly, this is a comprehensive report for perovskite-based WLEDs and would provide a new pathway toward low cost, high product yield, and highly efficient perovskites applicable for high-performance WLEDs. We anticipate that further improving the stability of perovskite at high temperature, which will make more leaps and bounds in perovskite phosphors-based WLEDs.

Conflicts of interest

There are no conflicts to declare.

Acknowledgements

The authors are grateful for the financial support from the Project of Scientific Foundation of Returned Overseas Scholars by Heilongjiang Province (LC2017030) and Key Project of Scientific Foundation by Heilongjiang Province (JJ2018ZZ0010).

References

1 W. Zhang, G. E. Eperon and H. J. Snaith, *Nat. Energy*, 2016, **1**, 16048–16055.
2 P. Li, L. Tan, L. Wang, J. Zheng, M. Peng, Y. Wang and H. Guo, *J. Am. Ceram. Soc.*, 2016, **99**, 2029–2034.
3 Y. Wang, K. Wang, Z. Han, Z. Yin, C. Zhou, F. Du, S. Zhou, P. Chen and Z. Xie, *J. Mater. Chem. C*, 2017, **5**, 9629–9637.
4 P. Von Dollen, S. Pimputkar and J. S. Speck, *Angew. Chem., Int. Ed.*, 2014, **53**, 13978–13980.
5 D. J. Wang, L. Xu, T. C. Gu, L. Ma and H. M. Zhang, *Rare Met. Mater. Eng.*, 2008, **37**, 1656–1659.
6 H. Y. Fu, X. S. Qiao, S. Cui, Q. Luo, J. Y. Qian, X. P. Fan and X. H. Zhang, *Mater. Lett.*, 2012, **71**, 15–17.
7 S.-Y. Kwak, S. Yang, N. R. Kim, J. H. Kim and B.-S. Bae, *Adv. Mater.*, 2011, **23**, 5767–5772.
8 I. O. Huyal, U. Koldemir, T. Ozel, H. V. Demir and D. Tuncel, *J. Mater. Chem.*, 2008, **18**, 3568–3574.
9 Q. Gong, Z. Hu, B. J. Deibert, T. J. Emge, S. J. Teat, D. Banerjee, B. Mussman, N. D. Rudd and J. Li, *J. Am. Chem. Soc.*, 2014, **136**, 16724–16727.
10 X. Chen, F. Zhang, Y. Ge, L. Shi, S. Huang, J. Tang, Z. Lv, L. Zhang, B. Zou and H. Zhong, *Adv. Funct. Mater.*, 2018, **28**, 1706567–1706573.
11 Q. Shan, J. Song, Y. Zou, J. Li, L. Xu, J. Xue, Y. Dong, B. Han, J. Chen and H. Zeng, *Small*, 2017, **13**, 1701770–1701794.
12 Y. H. Song, S. H. Choi, W. K. Park, J. S. Yoo, S. B. Kwon, B. K. Kang, S. R. Park, Y. S. Seo, W. S. Yang and D. H. Yoon, *Sci. Rep.*, 2018, **8**, 2009–2014.
13 X. Chen, D. Chen, J. Li, G. Fang, H. Sheng and J. Zhong, *Dalton Trans.*, 2018, **47**, 5670–5678.
14 J. C. Yu, J. H. Park, S. Y. Lee and M. H. Song, *Nanoscale*, 2019, **11**, 1505–1514.
15 S. Yang, W. Niu, A.-L. Wang, Z. Fan, B. Chen, C. Tan, Q. Lu and H. Zhang, *Angew. Chem., Int. Ed.*, 2017, **56**, 4252–4255.
16 D. H. Park, J. S. Han, W. Kim and H. S. Jang, *Dyes Pigm.*, 2018, **149**, 246–252.
17 L. Zhou, K. Yu, F. Yang, J. Zheng, Y. Zuo, C. Li, B. Cheng and Q. Wang, *Dalton Trans.*, 2017, **46**, 1766–1769.
18 J. P. Park, T. K. Lee, S. K. Kwak and S. W. Kim, *Dyes Pigm.*, 2017, **144**, 151–157.
19 B. Saparov and D. B. Mitzi, *Chem. Rev.*, 2016, **116**, 4558–4596.
20 G. Chen, W. Lin, H. Chen and T. Guo, *Mater. Des.*, 2019, **181**, 108100–108106.
21 A. Pan, B. He, X. Fan, Z. Liu, J. J. Urban, A. P. Alivisatos, L. He and Y. Liu, *ACS Nano*, 2016, **10**, 7943–7954.
22 S. Sun, D. Yuan, Y. Xu, A. Wang and Z. Deng, *ACS Nano*, 2016, **10**, 3648–3657.
23 X. Li, Y. Wu, S. Zhang, B. Cai, Y. Gu, J. Song and H. Zeng, *Adv. Funct. Mater.*, 2016, **26**, 2435–2445.
24 Y. Wang, D. Yu, Z. Wang, X. Li, X. Chen, V. Nalla, H. Zeng and H. Sun, *Small*, 2017, **13**, 1701587–1701594.
25 A. Swarnkar, R. Chulliyil, V. K. Ravi, M. Irfanullah, A. Chowdhury and A. Nag, *Angew. Chem., Int. Ed.*, 2015, **54**, 15424–15428.
26 L. N. Quan, R. Quintero-Bermudez, O. Voznyy, G. Walters, A. Jain, J. Z. Fan, X. Zheng, Z. Yang and E. H. Sargent, *Adv. Mater.*, 2017, **29**, 1605945–1605950.
27 J.-H. Cha, J. H. Han, W. Yin, C. Park, Y. Park, T. K. Ahn, J. H. Cho and D.-Y. Jung, *J. Phys. Chem. Lett.*, 2017, **8**, 565–570.

28 Q. Wang, W. Wu, R. Wu, S. Yang, Y. Wang, J. Wang, Z. Chai and Q. Han, *J. Colloid Interface Sci.*, 2019, **554**, 133–141.

29 Y. M. Chen, Y. Zhou, Q. Zhao, J. Y. Zhang, J. P. Ma, T. T. Xuan, S. Q. Guo, Z. J. Yong, J. Wang, Y. Kuroiwa, C. Moriyoshi and H. T. Sun, *ACS Appl. Mater. Interfaces*, 2018, **10**, 15905–15912.

30 M. I. Saidaminov, J. Almutlaq, S. Sarmah, I. Dursun, A. A. Zhumekenov, R. Begum, J. Pan, N. Cho, O. F. Mohammed and O. M. Bakr, *ACS Energy Lett.*, 2016, **1**, 840–845.

31 Q. A. Akkerman, A. L. Abdelhady and L. Manna, *J. Phys. Chem. Lett.*, 2018, **9**, 2326–2337.

32 J. Xu, W. Huang, P. Li, D. R. Onken, C. Dun, Y. Guo, K. B. Ucer, C. Lu, H. Wang, S. M. Geyer, R. T. Williams and D. L. Carroll, *Adv. Mater.*, 2017, **29**, 1703703–1703712.

33 Q. J. Han, W. Z. Wu, W. L. Liu, Q. X. Yang and Y. Q. Yang, *Opt. Mater.*, 2018, **75**, 880–886.

34 Q. Wang and W. Wu, *Opt. Lett.*, 2018, **43**, 4923–4926.

35 H. Yang, Y. Zhang, J. Pan, J. Yin, O. M. Bakr and O. F. Mohammed, *Chem. Mater.*, 2017, **29**, 8978–8982.

36 Y. Ling, L. Tan, X. Wang, Y. Zhou, Y. Xin, B. Ma, K. Hanson and H. Gao, *J. Phys. Chem. Lett.*, 2017, **8**, 3266–3271.

37 F. Zhang, H. Zhong, C. Chen, X.-g. Wu, X. Hu, H. Huang, J. Han, B. Zou and Y. Dong, *ACS Nano*, 2015, **9**, 4533–4542.

38 V. D. Kulakovskii, G. Bacher, R. Weigand, T. Kümmell, A. Forchel, E. Borovitskaya, K. Leonardi and D. Hommel, *Phys. Rev. Lett.*, 1999, **82**, 1780–1783.

39 N. Talebian, S. M. Amininezhad and M. Doudi, *J. Photochem. Photobiol., B*, 2013, **120**, 66–73.

40 F. Gabelloni, F. Biccari, G. Andreotti, D. Balestri, S. Checcucci, A. Milanesi, N. Calisi, S. Caporali and A. Vinattieri, *Opt. Mater. Express*, 2017, **7**, 4367–4373.

41 D. Zhou, R. Sun, W. Xu, N. Ding, D. Li, X. Chen, G. Pan, X. Bai and H. Song, *Nano Lett.*, 2019, **19**, 6904–6913.

42 K. Lin, J. Xing, L. N. Quan, F. P. G. de Arquer, X. Gong, J. Lu, L. Xie, W. Zhao, D. Zhang, C. Yan, W. Li, X. Liu, Y. Lu, J. Kirman, E. H. Sargent, Q. Xiong and Z. Wei, *Nature*, 2018, **562**, 245–248.

43 M. He, S. Liu, L. Ding, Z. Zhang, J. Liu, W. Xiang and X. Liang, *J. Am. Ceram. Soc.*, 2019, **102**, 930–935.

44 Z. Bao, H.-C. Wang, Z.-F. Jiang, R.-J. Chung and R.-S. Liu, *Inorg. Chem.*, 2018, **57**, 13071–13074.

45 G. Yang, Q. Fan, B. Chen, Q. Zhou and H. Zhong, *J. Mater. Chem. C*, 2016, **4**, 11387–11391.

46 H. Huang, Q. Xue, B. Chen, Y. Xiong, J. Schneider, C. Zhi, H. Zhong and A. L. Rogach, *Angew. Chem., Int. Ed.*, 2017, **56**, 9571–9576.

47 S. Lou, T. Xuan, C. Yu, M. Cao, C. Xia, J. Wang and H. Li, *J. Mater. Chem. C*, 2017, **5**, 7431–7435.

48 G. Li, H. Wang, T. Zhang, L. Mi, Y. Zhang, Z. Zhang, W. Zhang and Y. Jiang, *Adv. Funct. Mater.*, 2016, **26**, 8478–8486.

49 H. Huang, B. Chen, Z. Wang, T. F. Hung, A. S. Susha, H. Zhong and A. L. Rogach, *Chem. Sci.*, 2016, **7**, 5699–5703.

50 M. Yang, H.-s. Peng, F.-l. Zeng, F. Teng, Z. Qu, D. Yang, Y.-q. Wang, G.-x. Chen and D.-w. Wang, *J. Colloid Interface Sci.*, 2018, **509**, 32–38.

51 C. Sun, Y. Zhang, C. Ruan, C. Yin, X. Wang, Y. Wang and W. W. Yu, *Adv. Mater.*, 2016, **28**, 10088–10094.

52 Y. Hua, S. K. Hussain and J. S. Yu, *Ceram. Int.*, 2019, **45**, 18604–18613.